Cosmogenic nuclide-derived downcutting rates of canyons within large limestone plateaus of southern Massif Central (France) reveal a different regional speleogenesis of karst networks

Oswald Malcles, Philippe Vernant, David Fink, Gaël Cazes, Jean-François Ritz, Toshiyuki Fujioka, Jean Chéry

Earth Surf. Dynam., 12, 679–690, 2024
https://doi.org/10.5194/esurf-12-679-2024

Earth Surface Dynamics
Open Access
EGU

Cosmogenic nuclide-derived downcutting rates of canyons within large limestone plateaus of southern Massif Central (France) reveal a different regional speleogenesis of karst networks

Oswald Malcles[1], Philippe Vernant[1], David Fink[2], Gaël Cazes[1], Jean-François Ritz[1], Toshiyuki Fujioka[3], and Jean Chéry[1]

[1]Géosciences Montpellier, Université de Montpellier, CNRS, Montpellier, France
[2]Australian Nuclear Science and Technology Organisation, Sydney, Australia
[3]Centro Nacional de Investigación sobre la Evolución Humana (CENIEH), Burgos, Spain

Correspondence: Oswald Malcles (oswald.malcles@umontpellier.fr)

Received: 18 April 2023 – Discussion started: 23 June 2023
Revised: 16 February 2024 – Accepted: 6 March 2024 – Published: 7 May 2024

Abstract. We present 35 new burial ages (27 sites) based on ^{26}Al / ^{10}Be ratios of terrestrial cosmogenic radionuclides measured in clasts and sediments deep within 12 caves in the southern Massif Central, France. Our results, together with previously published burial ages, verify that cave morphogenesis has been continuously active in this region for at least the past ~ 6 Myr. Combining sample burial ages with their associated cave elevation above the modern stream bed gives a mean regional incision rate of $88 \pm 5\,m\,Ma^{-1}$ for the Grands Causses area. South of the Cevennes Fault Zone bordering the Grands Causses, the incision rate is $43 \pm 5\,m\,Ma^{-1}$, suggesting that this difference might be accommodated by the fault zone. Sediment burial ages from caves which are not located on river valley flanks or cliff walls are surprisingly too young compared to their expected ages when calculated using this regional average river incision rate. This suggests that the classical epigenic speleogenesis model that presumes a direct correlation between cave level development and regional base level lowering does not apply for the study area. Therefore, we propose that regional speleogenesis is mainly controlled by the removal of ghost rocks by headward erosion from river canyons to central parts of the plateaus, emptying incipient primokarst passages to create cave systems. Our results suggest a continuum process from hypogene primokarst composed of passages filled with ghost rock to one of epigene karst dynamics emptying these passages and creating cave networks. We propose that these processes are the major mechanism in the southern Massif Central that initiates speleogenesis and controls the geometry of the networks. In this region, tiered karst cannot be associated with the pace of incision of the major rivers but must be explained by former ghost rock (or hypogene) processes.

1 Introduction – the origin of caves

Speleogenesis has been an ongoing research topic for decades and debate on the spatial and temporal evolution of caves is equally as old (Palmer, 2017). The current paradigm of epigenic speleogenesis (Fig. 1) includes (1) steep vadose upstream sections converging into (2) phreatic or epiphreatic sub-horizontal passages constrained by the local water table and (3) subsequent groundwater emergence as springs at the river valley floor (e.g., Ford and Williams, 2007; Audra and Palmer, 2013; Harmand et al., 2017). In this epigenic model, the sub-horizontal passages, called cave levels or tiered karst, are assumed to have been created by dissolution of bedrock during a prolonged period of base level river stability. When river incision resumes, both the contemporary base level and water table lower, allowing formation of

new passages, while the previous generation of cave levels (usually higher in elevation) is isolated from further fluvial occupation. Therefore, each cave level is considered to reflect a base level at a certain period of time in the past. This broadly accepted correlation between the elevation of successive horizontal cave passages and river valley evolution is commonly used to study speleogenesis and quantify incision rates (e.g., Granger et al., 1997, 2001; Stock et al., 2005; Haeuselmann et al., 2007; Harmand et al., 2017). The complication with this simple view of the epigenic speleogenesis paradigm (ESP) is that although groundwater discharge dissolves carbonates, it also simultaneously physically erodes and transports insoluble residues from bedrock sections. This process implies that large enough passages must exist prior to speleogenesis onset of sub-horizonal cave levels to avoid the clogging of passages by insoluble bedrock fragments. To get around this problem, the conventional model implicitly assumes that, for most of the time, the open fractures in bedrock allow the removal of soluble and insoluble products and at the same time facilitating speleogenesis (in-depth discussions about the implications of the chemical weathering and mechanical erosion processes can be found in Dubois et al., 2014, or Quinif, 2010, for example). Other models have been proposed to explain speleogenesis, but they are commonly viewed as marginal processes "because these types of speleogenesis are not connected to a fluvial base level" (Harmand et al., 2017). They include hypogenic cave formation mainly due to confined deep groundwater with a dissolution potential not related to surface processes (e.g., Klimchouk, 2012) or ghost rock karstification (e.g., Dubois et al., 2014). Ghost rock karstogenesis (also called phantomization) was first described by Schmidt (1974) but mostly overlooked as a major karstification process, and according to Klimchouk (2017), it is a specific manifestation of hypogenic karstification. For others (e.g., Quinif, 2010; Dubois et al., 2014; Rodet, 2014) phantomization can be a major regional karstification process involving a first stage of bedrock chemical weathering along the least flow-resistant paths (e.g., faults, fractures, and bedding planes), with the subsequent removal of the soluble matrix under low hydrodynamic conditions leaving the rock structure with the more resistant insoluble matrix essentially preserved. During the first phase, which is limited to chemical weathering, only incipient passages are formed along weak flow paths (i.e., "ghost-like" karstification), though they can often be misinterpreted as cave sediment deposits. The progressive alteration of the rock – the ghost weathering process – leads to interconnection of ghost rock zones. This network of connected ghost rock zones, which Rodet (2014) defines as "primokarst", is the incipient geometry along which cave networks will eventually develop, depending on hydrodynamic conditions during the speleogenesis phase. Indeed, if hydrodynamic conditions change, allowing rapid water flow, the mechanical erosion of the ghost rock will then preferentially open these weaker pre-existing paths and create caves.

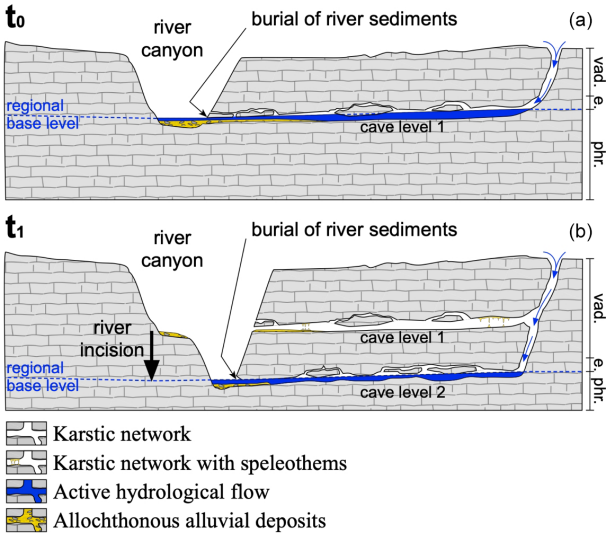

Figure 1. Cave level development accordingly to the commonly accepted epiphreatic speleogenesis paradigm (ESP). Panel **(a)** (at $t = t_0$) shows how water entering from the plateau dissolves and creates steep passages in the vadose zone (vad.) to connect to the epiphreatic (e.) and phreatic (phr.) zones, where it forms subhorizontal passages linked to the regional base level. Panel **(b)** (at $t = t_1$) shows how the subsequent river incision lowers the water table and creates new cave levels (level 2) at the regional base level. Previously formed (older) cave levels (level 1) become abandoned.

Whatever model of karstification is chosen, the passage formation is the result of the following three steps (e.g., Klimchouk, 2015): (1) the early stage corresponds to the widening of the flow pathways or primokarst formation; (2) the breakthrough phase which can be seen as the formation of efficient passages where the water can flow quickly and easily; and (3) the last phase is when the main drains are well established, allowing the stabilization of the system and the growth of the principal conduits. The main difference between the epigene karstification and the other processes is the relation to the regional base level. Epigene karst geometry is directly related to the river incision dynamic, while hypogenic and ghost rock karstification occur below the base level, and subsequent tiered karst geometries cannot be interpreted in terms of river entrenchment phases. Indeed, the ghost rock formation is considered to occur principally below the base level, with a low-energy water flow exporting soluble elements without exporting the insolubles. This period of localized alteration creates geometries including horizontal primokarst passages. When the primokarst passages are ripped open by the valley entrenchment, water can freely flow through the newly formed opening, allowing hydrodynamic conditions to change to high energy and export ghost rocks while emptying the primokarst network and forming cave passages with eventual horizontal galleries. This model does not need river level steadiness. We assume that most of the time the intersection of the primokarst by the topogra-

phy is related to the entrenchment of the river, but other processes, such as escarpment recession for example, could also provide a physically satisfactory explanation. The process of headward ghost rock drain and subsequent cave creation has been observed in real time in Belgian quarries (e.g., Quinif, 2010; Dubois et al., 2014). Erosion of the ghost rock can occur below the base level, as long as the hydrological gradient is sufficient to create a high enough energy water flow to permit the export of the insolubles. Large water flow loops at depth have been proposed to explain some hypogene cases since the flow is upward on one end of the loop (Klimchouck, 2017). Dandurand et al. (2019) refer to a similar process with the large convection cells of water at depth to explain ghost rock formation and its subsequent drain, sometimes creating a deep sump at more than 100 m below the base level. In this model, deep convective cells are proposed as a satisfactory explanation for primokarst formation, subsequent drain, and finally deep phreatic loops such as Fontaine-de-Vaucluse or Touvre springs.

In this study, we investigate speleogenesis of the Grands Causses region in the southern Massif Central, France (Fig. 2). We apply the pioneering methods of Granger et al. (1997), using terrestrial cosmogenic radionuclide (TCN) ^{26}Al / ^{10}Be ratios to estimate burial ages of quartz-rich sediment and quartz cobble cave infill, together with detailed cave mapping to quantify river incision rates. We spatially distinguish burial ages between caves opened on river canyon walls to those centrally located in plateaus to test the above models. Our results challenge the pervasive current ESP model of speleogenesis.

2 Geology and Plio-Quaternary geomorphologic evolution of the Grands Causses

The Grands Causses region (Fig. 2) is a large, elevated plateau of thick sub-horizontal Mesozoic carbonated series overlying a Hercynian metamorphic and plutonic crystalline basement. Mean surface elevation is around 800 m above sea level (a.s.l.), and its southeastern margin is defined by a steep slope along the Cevennes Fault Zone (CFZ). The latest activity of this Hercynian-inherited major fault system, according to Séranne et al. (2002), is an uplift of the northwestern sector during the Serravallian/Tortonian (prior to ca. 8 Ma). Several rivers have their upper riverbeds and sources within crystalline areas (granite and schists). Their lower riverbeds carve deeply into the limestones on their journey to the Mediterranean Sea or the Atlantic Ocean, sculpting canyons that can be up to 400 m deep (Fig. 2). Incision rates and timing of canyon formation are still debated. Since the early 2000s, it has generally been considered that the Grands Causses morphology was mostly inherited from the Miocene without significant incision later during the Quaternary (Séranne et al., 2002). Recent quantification of incision rates based on TCN burial dating in caves of the Rieutord river yielded rates of $\sim 80\,\mathrm{m\,Ma^{-1}}$ over the last ~ 2 Myr (Malcles et al., 2020a) on the Mediterranean side and 40 to $120\,\mathrm{m\,Ma^{-1}}$ for the Jonte River on the Atlantic side over the last ~ 8 Myr (Sartégou et al., 2018).

3 Methods

3.1 Terrestrial cosmogenic nuclide (TCN) data

We use TCN burial ages to quantify regional incision rates. The method (Granger et al., 1997) is based on the change in the initial ^{26}Al / ^{10}Be ratio produced by cosmic ray bombardment of subaerially exposed rocks, whereby after erosion and via fluvial transport, the irradiated quartz-rich grains or cobbles are deposited and stored in cave systems. If burial is at a sufficient depth (such as the case in our study), production ceases, and the measured ^{26}Al / ^{10}Be sample ratio is reduced compared to its initial ratio due to differential decay of the shorter-lived ^{26}Al (half-time of 1.387 and 0.705 Myr for ^{10}Be and ^{26}Al, respectively; Korschinek et al. (2010); Chmeleff et al. (2010)). We sampled quartz-rich alluvium and small cobbles in 8 new caves and resampled 4 from caves previously reported (Malcles et al., 2020a, b) for a total of 35 samples. In order to provide a strong constraint in calculating river incision rates, we sampled, where possible, tiered caves that show horizontal galleries. The selection of caves to sample was made based on morphological evidence as, for example, in the Scorpions caves that shows all the indices of being an endokarstic loop and by published work (Camus, 2003). 3D cave topography can be obtained from the KARST3D database (Team KARST3D, 2019). The inventory of river canyons in this work includes three new Mediterranean Sea tributaries (the Hérault, Arre, and Vis rivers) and a fourth canyon, the Rieutord, which was resampled (Malcles et al., 2020a).

The samples were crushed, sieved, and processed with several selective chemical dissolutions to obtain pure quartz (Khol and Nishiizumi, 1992; Child et al., 2000). After final hydrofluoric acid (HF) etchings, the samples were dissolved in full-strength HF with the addition of $\sim 250\,\mu$g of a Be carrier solution derived from beryl mineral with a ^{9}Be concentration assayed via inductively coupled plasma mass spectrometry (ICP-MS) to $\pm 1\,\%$ in concentration. Be and Al were then separated by ion exchange chromatography and selective pH precipitations. Final BeO and Al_2O_3 powders were mixed with Nb and Ag, respectively, and measured, using the SIRIUS Accelerator Mass Spectrometer (AMS) facility at ANSTO (Australia's Nuclear Science and Technology Organisation) in Sydney, Australia (Wilcken et al., 2019). All AMS results in this study were normalized to standards of KN-5-4 and KN-4-4 for Be and Al, respectively (Nishiizumi et al., 2007), and corrected for background using the set of procedural chemistry blank samples prepared in each batch of 10 samples. Final uncertainties for ^{10}Be and ^{26}Al concentrations include AMS statistics, 2 % (Be) and 3 % (Al)

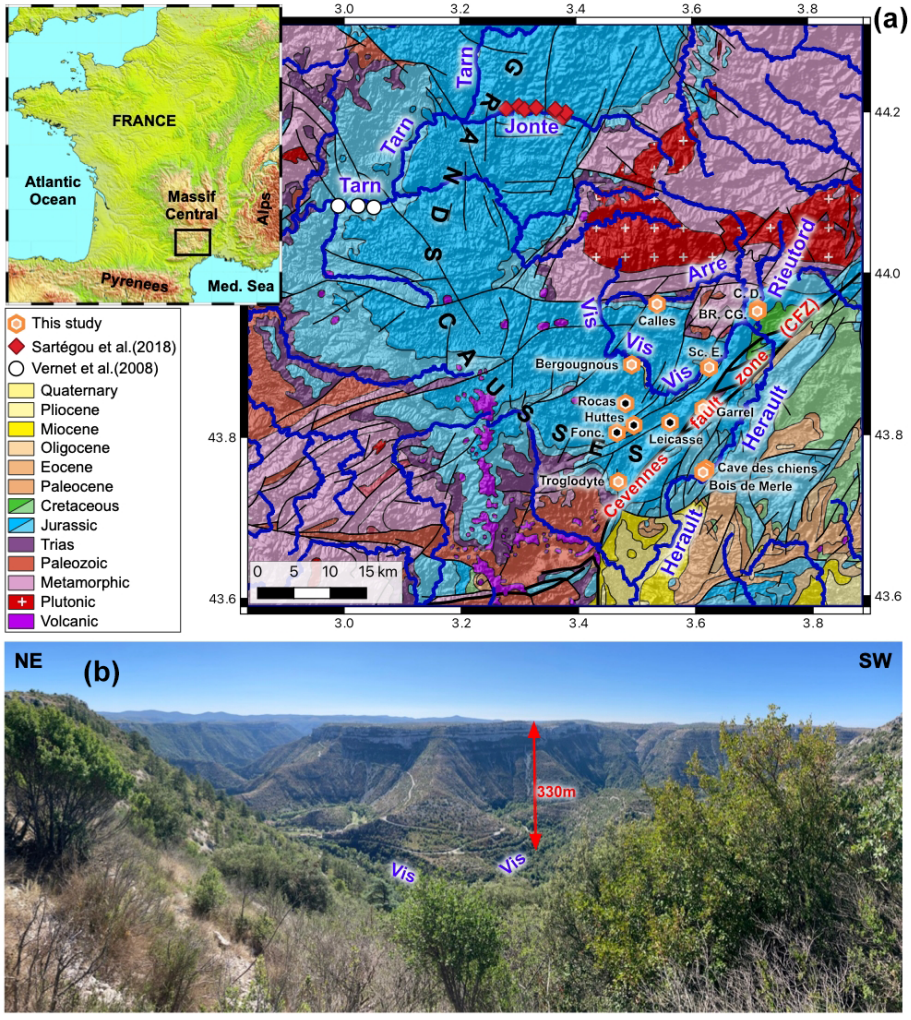

Figure 2. **(a)** Simplified geological map of the study area and sample locations. The metamorphic and plutonic bedrock provide quartz-rich sediments to the Tarn, Jonte, Arre, Rieutord, Vis, and Hérault rivers. For the Jurassic and Cretaceous rocks, darker colors indicate thick limestone formations, while lighter colors are for marls and thin limestone formations. Symbols with black hexagons (Fonc, Huttes, Rocas, and Leicasse) indicate sampled caves located away from the river canyons within a central section of the plateau. Sc. is for Scorpions, E. is for Escoutet, BR. is for Bord de Route, CG. is for Camp de Guerre, C. is for Cuillère, D. is for Dugou, and Fonc. is for Fonctionnaire. **(b)** Photograph of the Vis river canyon located next to the Bergougnous sample.

standard reproducibility, 1 % uncertainty in the Be carrier solution concentration, and a representative 4 % uncertainty in the natural Al measurement made by inductively coupled plasma optical emission spectrometry (ICP-OES) in quadrature.

All sample identification, location, and elevation (relative to modern base level), with their ^{10}Be and ^{26}Al concentrations and associated fully propagated analytical errors, are given in the Supplement (Table S1). Two samples were repeated as a check on the internal consistency of the processing and AMS measurement.

3.2 Burial age modeling and paleo-erosion rates

When large enough cobbles were available ($> \sim 100$ g), we independently processed them to obtain several burial ages for the same alluvium layer (Scorpions, Escoutet, and Leicasse caves). An alternate approach is to use the isochron method (Balco and Rovey, 2008) which is, usually, expected to provide a more reliable age determination, as it can accommodate the variability in pre-burial exposure history of cobbles. This method allows the removal of the differences in the initial or inherited ^{10}Be and ^{26}Al concentrations (which result from variations in the erosional equilibrium conditions of source bedrock, etc.) from the final measured cosmogenic nuclide inventories, with the a priori assumption that post burial production was the same for all isochron samples. This

method is valid as long as all of the measured samples maintained the same depths below the surface immediately following deposition in the cave system. In other cases, where only smaller elements could be found in the same deposit, we decided to process the samples as amalgamates with at least ~ 200 g of quartz at the beginning of the treatment. The latter approach provides an average concentration and hence an average burial age.

Details on the burial dating theory are given in several studies (e.g., Granger et al., 1997; Granger and Muzikar, 2001; Dunai, 2010). We performed a two-step grid search to find the combination of burial ages and paleo-denudation rates (obtained based on a sea level high latitude (SLHL) $^{26}\mathrm{Al}/^{10}\mathrm{Be}$ production rate ratio of 6.61 with spallation SLHL production rate of 4.47 and 30.29 atm $\mathrm{g}^{-1}\,\mathrm{yr}^{-1}$ for ^{10}Be and ^{26}Al, respectively)) which are consistent with the measured ^{10}Be and ^{26}Al concentrations. In the first step, we used a loose grid with burial ages ranging from 10 kyr to 10 Myr, with 1000 values spaced evenly on a log scale, and paleo-denudation rates from 0.1 to 1000 m Ma^{-1} with 200 values also spaced evenly on a log scale. We check if the obtained values for ^{10}Be are consistent with ^{26}Al; if not, the concentrations are considered inconsistent, with a simple history of bedrock erosion followed by the river transport and finally the burial in a cave. In this case, no burial age can be estimated. If a consistent set of values exists, then we perform a second grid search, which is similar to the first one but with tighter intervals to compute the consistent set of burial ages and paleo-denudation rates. To compute the theoretical concentrations, we account for variability in the cosmic-ray flux as a function of elevation and latitude and therefore the cosmogenic nuclide production using scaling factors. These scaling factors use the sampling site parameters (e.g., elevation). For the neutron spallation contribution to production, we use the Lal (1991) scaling factors. For the muon contribution, we do not use slow and fast muon production rate scaling factors (as per Braucher et al., 2013) but rather use the simpler geographic scaling method, as described in Balco (2017). The best combination of burial age and paleo-denudation rate is the one leading to the smallest residual (i.e., the difference) between the measured and computed ^{10}Be and ^{26}Al concentrations; we do so using the lowest chi-squared value of the residuals computed for all parameters of the grid. The obtained values are plotted in Fig. 3 and given in the Supplement (Table S1). Both the minimal and maximal combination of burial age and erosion rate providing modeled concentrations in the range of the measured one ($\pm 1\sigma$) are computed to estimate uncertainties. The upper uncertainty and the lower uncertainty are the distance between the best estimation and the maximal acceptable age and erosion rate or the minimal acceptable age and erosion rate.

4 Results and discussion

In Fig. 3, we present the burial ages from this study plotted against the cave elevation for each burial sample relative to local base level. Figure 3 also includes paired burial age–elevation pairs from previous TCN studies of Sartégou et al. (2018) for the Jonte and Tarn rivers, from Malcles et al. (2020a) for Rieutord, and optically stimulated luminescence (OSL) results for terraces of the Tarn river from Vernet et al. (2008). For cave samples directly associated with the flanks of river canyons, the elevation is relative to the modern river channel, while for cave samples within central plateau regions, the nearest river defines the relative elevation of the sample compared to local base level.

4.1 Burial ages

The new suite of burial ages spans the time range of the method from a few hundreds of thousands of years (e.g., Fonctionnaire cave) to slightly more than 5 Myr (Troglodyte and Huttes caves). Three different populations of ages are obtained (Fig. 3) which are spatially correlated but do not obey a common age–elevation relationship.

First, the three cave systems associated with the Vis river canyon (Scorpions, Bergougnous, and Escoutet) provide relatively young ages ranging from ~ 0.8 to 1.3 Ma while being located no more than 120 m above the local river level. The results for these samples present, at the first order, the same age–elevation relationship for river incision of about 85 m Myr that was previously published for the caves of the Rieutord river canyon (Malcles et al., 2020a). This age–elevation relationship is also obtained for the slightly older samples from the Calles cave (amalgams) that range from 1.9 to 2.8 Ma and are located ~ 200 m above the Arre riverbed. Finally, the ~ 5.4 M and +435 m of the Troglodyte cave deposit is also in very good agreement with this relationship. For some of these caves, multiple cobbles were processed for the same site. Isochron and amalgamate analyses were performed for Scorpions and Escoutet, and only amalgamate samples were taken for Calles and Bergougnous. We suggest that the youngest burial age from the deposit is expected to be the best estimate of the timing before the cave becomes isolated or disconnected from further fluvial occupation due to the river entrenchment. This item is further discussed in Sect. 4.2.

Second, samples from Garrel, Cave des chiens, and Bois de Merle, which are shown as black filled data symbols in Fig. 3, have burial ages that are too old with respect to their given elevation when compared to the age–elevation trend discussed above. For example, the Cave des chiens is located at 142 m above the Hérault riverbed which would result in a calculated burial age for the alluvium deposits of around 1.5 Ma, while the measured burial age is $3.33\ ^{+0.59}/_{-0.48}$ Ma, suggesting a much lower age–elevation trend by up to a fac-

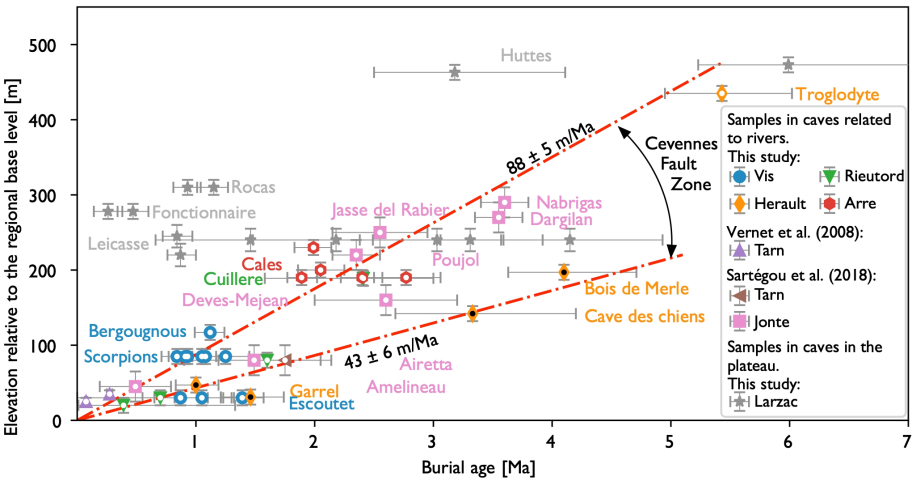

Figure 3. Burial age vs. relative elevation to the local water table level for each sample. Gray stars indicate caves that are not located on the flanks of the river channel but rather in central plateau areas; all the other caves are adjacent to or on river flanks or canyon walls. Jonte S. and Tarn S. are ^{26}Al / ^{10}Be results from Sartégou et al. (2018); Tarn V. are OSL results for Tarn river terraces from Vernet et al. (2008), and Rieutord shows ^{26}Al / ^{10}Be results from Malcles et al. (2020a). The average incision rate NW of the CFZ is calculated using samples represented by symbols with white circles inside, while the rate at the SE side of the CFZ is given by the data obtained at locations represented by symbols with black circles inside.

tor of ∼ 2. We will discuss this discrepancy in age–elevation trends in Sect. 4.3.

Finally, the large group of samples from the Rocas, Fonctionnaire, Huttes, and Leicasse caves, which are shown as gray filled data symbols in Fig. 3, present burial ages at odds with any age–elevation relationship previously presented. Indeed, some caves, while being amongst the highest relative to the river level (+310 m for Rocas and +278 m for Fonctionnaire) present unexpected young burial ages ($1.04^{+0.16}/_{-0.18}$ and 0.37 ± 0.18 Ma, respectively). Furthermore, multiple samples from exactly the same deposit of the Leicassse cave provide a very large age discrepancy (1.46 $^{+1.03}/_{-0.8}$ to 4.15 $^{+0.78}/_{-0.51}$ Ma). These unexpected results are discussed in Sect. 4.4.

4.2 Multiple samples in the same cave level

Depending on the cave, some individual burial ages are spread over a wide age range (e.g., Leicasse; Fig. 3). Due to being sampled in the same deposit, such cases are an indicator of a more complex history than the classical erosion–transport–burial model assumes. One explanation is that the wider the range, the more likely the sediments laid were partially buried in a sub-aerial alluvium surface layer before being buried in the cave later when the sediments were reworked. When we compute independent burial ages, we assume that the catchment-wide mean erosion rate of the paleobasin was sufficiently high to avoid significant variability in the initial ^{26}Al / ^{10}Be (inheritance) ratio. The use of the Balco and Rovey (2008) isochron method on these three sets of samples can be used to test this assumption. Without surprise, the samples with a limited dispersion in the individual burial age computations (Escoutet and Scorpions caves) show well-constrained linear regressions of ^{26}Al vs. ^{10}Be concentrations with $R^2 > 0.91$. On the other hand, samples from the Leicasse cave have a poor constraint with a regression coefficient of $R^2 < 0.2$. This is also consistent with the very large estimates of paleo-denudation rates for two of the five sampled cobbles in the Leicasse cave, which give inconsistent values compared to all other obtained paleo-denudation rates (< 50 m Ma^{-1}; Fig. 4). Omitting these two outliers, which we assume is related to a complex burial history, our results suggest no large variation in denudation rates over the last 4 Myr (Fig. 4). We recall that because of many uncertainties related to the paleo-denudation rate calculation (e.g., paleo-elevation of the sediment source) only the order of magnitude seems reasonable to be discussed. Therefore, rather than using the isochron method, we prefer to use the independent age estimates. This choice is also supported by our observations of alluvium layers of variable thicknesses (< 15 m) on the plateaus, and we advocate that the dispersion in the individual burial ages is related to the partial burial of the samples in these alluvium layers before being drained into the cave. Some would have endured partial or full burial (i.e., located within or at the bottom of the surface alluvium layer), while others would have stayed at the surface fully exposed. For the Leicasse cave samples, the conversion of TCN concentrations into burial ages is not straightforward. In this case, the younger age is a better measure, that is equal or older, of the true burial age (∼ 0.8 Ma) of the cave deposit, since its ^{26}Al / ^{10}Be initial ratio was the one least likely to have been perturbed. This sample with the younger age was then the one located closer to the surface in the sub-

aerial alluvium layer prior to its drain into the cave and a deep burial preventing ^{26}Al and ^{10}Be production. The older age (~ 4 Ma) is a better measure, that is equal or younger, of the emplacement of the surface alluvium layer that was subsequently buried in the cave. This sample was the one located the deepest in the surface alluvium layer before it was drained into the cave. We point out that these locations in the alluvium layer are relatives; that is to say, if it seems logical that the oldest is initially the deepest and the youngest is the shallowest, no causal link the absolute depth prior to the final burial, however, is unknown. A few constraints can be brought by the fact that the alluvium layer thickness is usually less than 15 m, according to the local geological map (Alabouvette et al., 1988) and also from our field observations, which is sufficient to result in a variety of cases where production totally ceased or was only partially reduced. All the other burial ages and associated excessively high paleo-denudation rates should be used with great caution (Fig. 4; Leicasse samples). Because of the direct cave entrances toward the Vis river channel, and the short distance (few hundreds of meters) between the sampling site and the cave entrances, the Scorpions and the Escoutet cave samples are less likely to be affected by the injection of previously deposited alluvium at the surface of the plateaus. The narrow dispersion of independent burial ages and paleo-denudation rates are consistent with this observation. Therefore, we suggest that in the case of burial age determination for cave alluviums, if several samples are collected, then independent ages should be computed, and the younger one should be retained, except if complications are expected due to the presence of glaciers in the valleys, which is not the case in the study area.

4.3 Incision rates and southern Cevennes Fault Zone activity

At first glance, Fig. 3 does not reveal any discernible patterns. However, when we rank the caves with respect to distance to the nearest river canyon and also their location in relation to the Cevennes Fault Zone (CFZ), three distinct sample subsets become apparent. The first one, the set of Larzac cave burial ages (Leicasse, Fonctionnaire, Rocas, and Huttes; gray symbols in Fig. 3), is located within the Larzac plateau (the southern plateau of the Grands Causses plateaus). All these caves are 2.5 to 5 km away from the nearest river channel and show no clear relationship between burial ages and relative elevations to the base level. We will discuss these caves in Sect. 4.4. With the Larzac caves set aside, all other cave burial ages (non-gray symbols) in Fig. 3 have cave entrances located in river channels when the base river level was close to the cave entrance elevation. These caves, located within the steep flanks of river channels, show a clear linear correlation – the higher the sample is above today's riverbed, the older its burial age (Fig. 3). The CFZ is a major geologic and topographic feature of the area. A first set of caves (Garrel, Bois de Merle, and Cave des chiens) resides southeast of the CFZ in a lower-elevation limestone plateau ~ 300 m a.s.l. (shown with black filled symbols in Fig. 3), while the second includes all the caves located in the Arre, Jonte, Rieutord, Tarn, and Vis river valleys and also the Troglodyte cave (white filled symbols in Fig. 3) and lies northwest of the CFZ in higher-elevation plateaus (600–1000 m a.s.l.). Using the cave location relative to the CFZ to define our two populations, we obtain an incision rate of 43 ± 6 (1σ; $n = 4$) m Ma^{-1} for the southeast, while all other samples to the northwest of the CFZ lead to an incision rate of 88 ± 5 m Ma^{-1} (1σ; $n = 32$) (see Fig. 3), consistent with the local previous estimates for the Jonte valley (Sartégou et al., 2018) and for the Rieutord samples (Malcles et al., 2020a). The low differential incision rate between the two populations of ~ 40 m Ma^{-1}, if focused on the CFZ, could lead to earthquakes with long recurrence times, consistent with the unexpected 2019 M_w 4.9 Teil earthquake (Ritz et al., 2020). Indeed, if we consider that the 40 m Ma^{-1} is the expression of a differential uplift rate localized on the CFZ, then the fault slip rate would be ~ 0.04 mm yr^{-1}. Using the classical relationships of Wells and Coppersmith (1994), this slip rate is expected to promote a M_w 6.5 earthquake with a ~ 10 kyr recurrence time, though a longer recurrence time or lower magnitude could be an equally plausible inference, for example, by taking a distributed slip rate along several faults of the CFZ. Further discussion of this observation is beyond the scope of this article, and a dedicated study focused on the CFZ activity should be conducted before drawing any robust conclusion. We point out, however, that this ~ 40 m Myr^{-1} of uplift differential is consistent with numerical models showing that the flexural response of the lithosphere due to erosional unloading (Malcles et al., 2020a) could explain this difference in the incision rates without the need for seismic ruptures on the CFZ.

4.4 Speleogenesis implications: headward erosion of altered rock zones

The unexpected result of diminished burial ages shown in Fig. 3 (when compared with the expected one using the regional trend of ~ 90 m Ma^{-1}) came from the four Larzac plateau caves that are at least 2.5 km away from any nearby river channel (Fig. 2 and gray filled symbols in Fig. 3). These caves have a clear classical tiered morphology that can be seen on the KARST3D database (Team KARST3D, 2019). Quartz-rich sediments in Rocas cave are only located -20 to -40 m deep below the surface (555–575 m a.s.l.), while the deepest part of the cave that is humanly accessible is at -130 m (465 m a.s.l.) (Fig. 5). In Fonctionnaire cave, the sediments are in the lowest of the three levels, at -75 m below the surface (520 m a.s.l.). In the Leicasse cave, which has 16 km of mapped passages, alluvium is deposited in a ~ 1 km long passage at more than -140 m below the surface (440 m a.s.l.). The five Leicasse quartz cobbles sampled in a common layer at ~ 455 m a.s.l. (coulée Borg deposit)

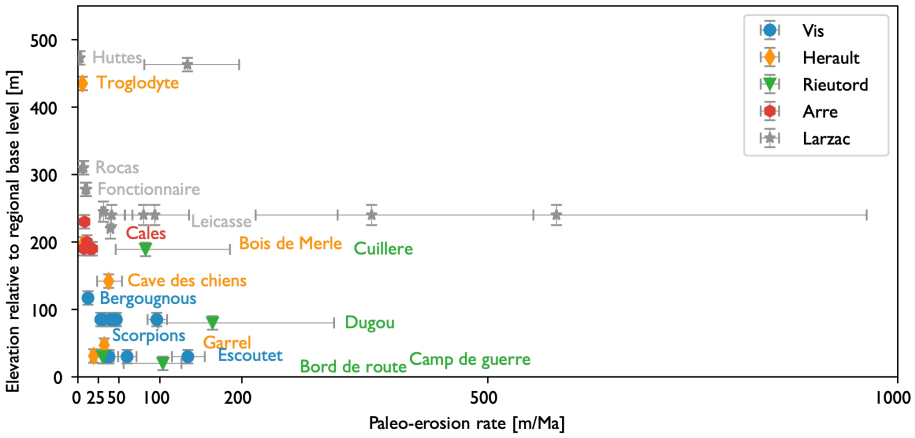

Figure 4. Paleo-erosion rate vs. relative elevation to the local water table level for each sample of this study. Caves not located on the flanks of the river channel but in central plateau areas are in gray, and all the other caves are adjacent to or on river flanks or canyon walls.

have burial ages ranging from 0.8 to 4.1 Ma. The Huttes cave is a 200 m long horizontal cave consisting of one level at 700 m a.s.l. Using the youngest burial age from each of the four caves as the closest age for sediment emplacement leads to burial ages inconsistent with that expected from epigenic speleogenesis paradigm (ESP), which would predict ages 2 to 4 Ma older – or alternatively, a cave level elevation 150 to 250 m lower than recorded compared to the regional base level at the time of the deposit (Fig. 3).

The absence of sediments below 40 m depth in Rocas cave indicates that the lower galleries formed less than a 1 Myr ago, after the emplacement of alluvium in the cave's highest level. In this younger part of the cave, passages show morphologies similar to those reported for ghost rock caves by Dubois et al. (2014) and Rodet (2014); that is to say, the cross sections of the galleries are characterized by lens (or half lens) shapes extending in the weathered strata, while the non-weathered strata and the lower parts of the galleries are characterized by scallops, potholes, and incised meanders. Furthermore, the preserved ghost rock at the type of the lens shape has porosities larger than 10 % (Fig. 5). In the ESP model, the meteoric water moves downwards through plateau bedrock, enlarging fractures and bedding planes to form the cave gallery at the contemporary base level. In contrast, the sub-horizontal upper level of the Rocas cave, which was filled with sediments 1 Myr ago, is clearly not related to the base level of the Vis river, located at that time 250 m lower, as registered by the same 1 Ma burial ages for the Scorpions and Bergougnous cave samples (Fig. 3). The same rationale applies to Fonctionnaire, Leicasse, and Huttes caves, and no impervious layers of marls are reported in the stratigraphic log at these cave elevations that could produce a perched karst. Furthermore, the wide range of the five cobble burial ages for the Leicasse (Fig. 3) and the paleo-denudation rates (Fig. 4) are significantly larger than the ranges for all the caves located within river channels (e.g., the five cobbles for Scorpions). We conclude that the sediments emplaced in Leicasse were not transported into the cave quickly or directly by riverine fluvial processes, but they had resided at shallow depth within sub-aerial alluvium layer at the surface of the plateau at least for a period of 3 Myr, which is the difference between the youngest and the oldest measured cave burial ages of the five samples. Alluvium of former poljes are present at the surface of the Larzac plateau and could be the source of the sediments that were later buried in the cave at the −140 m depth without a direct relation with the contemporary base level.

Based on these results, we propose that contrary to the ESP, the speleogenesis of the Larzac plateau is driven by karstic headward erosion from the canyon walls to the center of the plateau rather than by water working its way from the top of the plateau toward the valley. Given the rather quick formation of the caves, we propose that the passages were pre-structured by an alteration phase under a low hydrodynamic gradient leading to numerous incipient passages full of ghost rocks or isovolumic alterite, as schematically described in Fig. 6, retaining the original rock structure, and called primokarst (Rodet, 2014). Ghost rocks remain trapped in incipient passages where the water flow is practically absent since the boundaries of these incipient openings are impervious rocks, very thin fissures, or bedding planes allowing only water and ions to slowly flow through. When the canyon cuts through one of these passages, it opens an outlet large enough to create a high hydrodynamic gradient and allows the mechanical removal of the ghost rocks and the creation of a new cave in a fairly short time, as experienced in real time in Belgian quarries (Quinif, 2010). This is what occurred after 1 Ma for the lower part of the Rocas cave and around 0.3 to 0.5 Ma ago for the Fonctionnaire cave (Fig. 6). This headward erosion works its way from the canyon walls toward the center of the plateau following the primokarst structures and possibly creates deep sump (> 100 m) rather than a river-related tiered

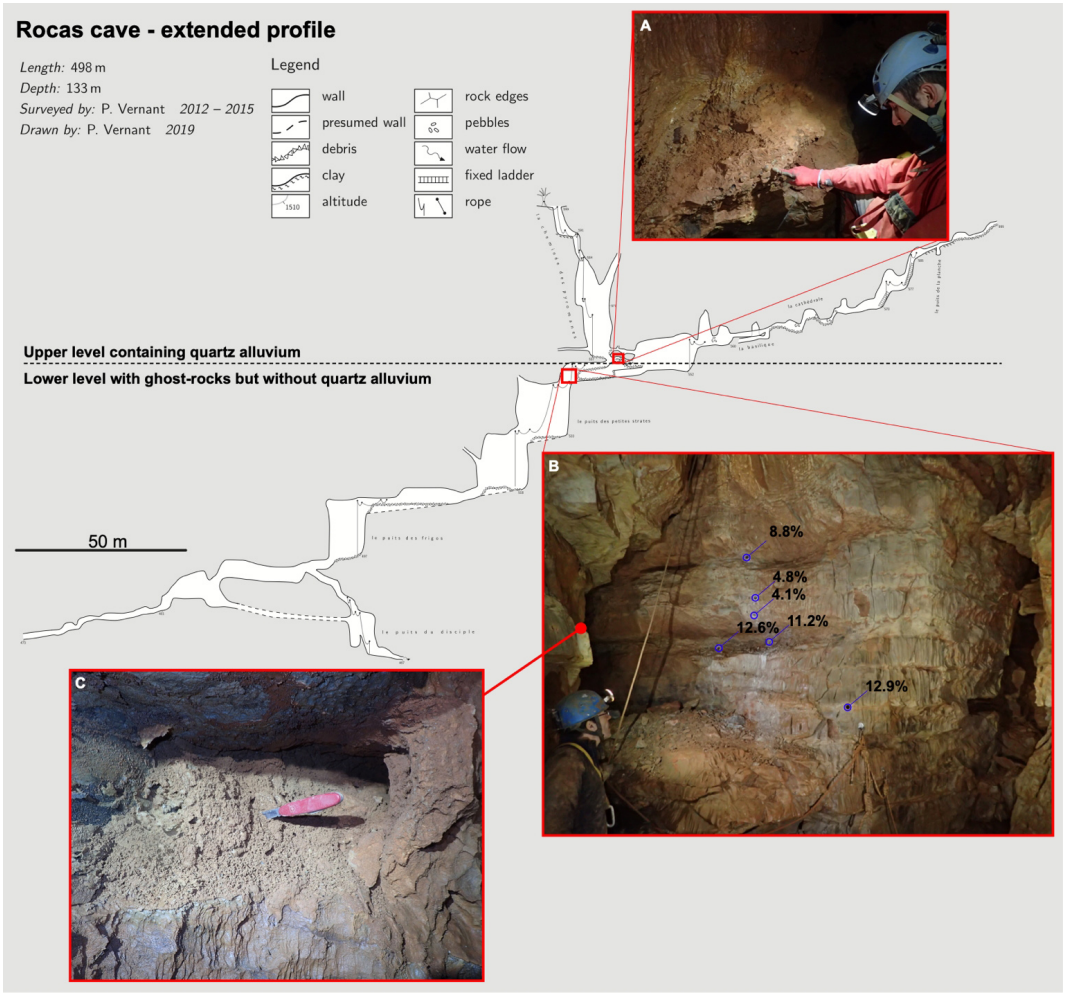

Figure 5. Extended profile of Rocas cave, with the lower limit of the upper level containing the quartz alluvium **(a)** and the lower level without quartz alluvium but with ghost rocks. Example of a cave wall with higher porosities near the beading planes showing the ghost rocks **(b)**. Sometimes the porosity is so high that the rock structure is still apparent but fully pulverulent **(c)**.

cave. Once the voids are opened, the water can flow through quickly and modify the cave morphology, enlarging it and creating hydrodynamic markers like scallops. The specificity of the Larzac plateau with sparse and thin deposits of quartz-rich alluvium across its surface has led to these unexpected results showing that cave levels, at least in this region, are related to preferential alteration levels that are subsequently emptied and, in some cases, enlarged by underground rivers when the primokarst was near or below the base level. While previous authors have already proposed that ghost rock removal could lead to large networks (Dubois et al., 2014; Quinif and Bruxelles, 2011), our results show that this process can be the major mechanism in the speleogenesis of large limestone plateaus like the Larzac (1000 km^2). These new observations also suggest that karstification can be a continuum process starting with hypogenic/ghost rock karstification and continuing with epigenic processes. The main difference in the ghost-like karstification compared to the widely accepted ESP model is that the network cave geometry is already established during a hypogene/ghost rock phase and that the evolution of the base level with its associated water gradient modification is a subsequent phase mostly responsible for the opening of the voids with little control on their structure. As pointed out by Dubois et al. (2022), karst morphologies are used by scientists to speculate on processes that induce speleogenesis. It leads to a tremendous number of different processes to form caves (see, for example, Fig. 3 in Harmand et al., 2017). Here we choose to follow an approach driven by the principle of parsimony, also termed Occam's razor, and propose a continuum process where cave geometry complexity is only driven by the primary phase of alteration. We are not the first authors to do so (e.g., Dubois et al., 2014, 2022) but acknowledge that this is an ongoing debate, as attested by the discussions with the reviewers triggered by the first drafts of this study. Quinif (2010) suggested the need for a new paradigm about karstogenesis implying ghost rock

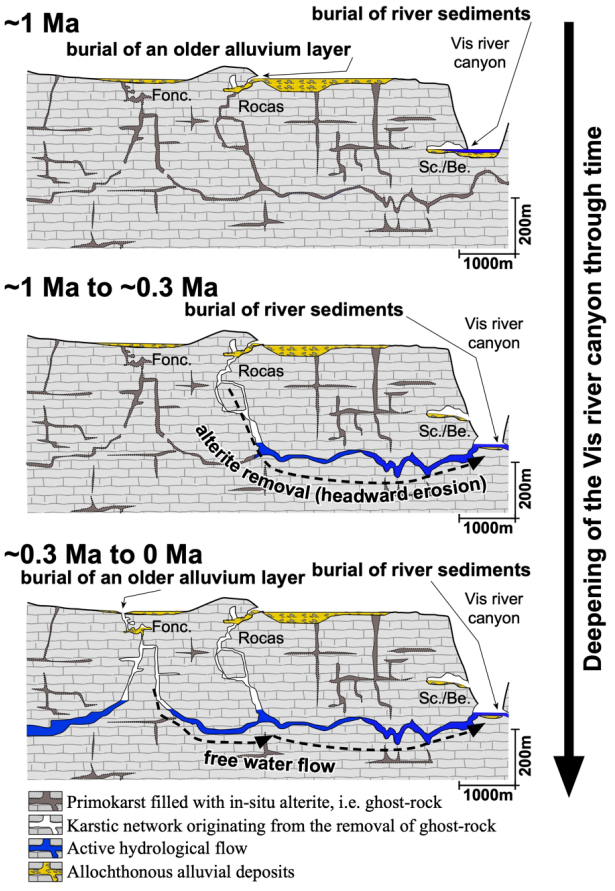

Figure 6. Proposed speleogenesis model for the cave in the center of the Larzac plateau based on the burial ages obtained in this study. The speleogenesis of the area is primarily due to alterite (ghost rock) removal due to underground headward erosion. Fonc. is for Fonctionnaire cave, and Sc./Be. are for Scorpions and Bergougnous caves.

processes. We know from the history of sciences that shifting from one paradigm to another is a complex journey (Kuhn, 1962). More studies and debates will be needed to overcome the present matter of contention about how ghost rock processes should be considered in karstogenesis: is it rather as a secondary process (e.g., Schmidt, 1974; Klimchouk, 2012) or the primary one (e.g., Rodet, 2014; Dubois et al., 2014, and the present study)?

5 Conclusions

Combining 22 new burial ages with 15 previously published ones, we propose a mean regional river incision rate of $88 \pm 5\,\mathrm{m\,Ma^{-1}}$ for the Grands Causses region and the first incision rate for the Hérault river of $43 \pm 6\,\mathrm{m\,Ma^{-1}}$, both over the last ~ 4 Myr. These two regions are separated by the Cevennes Fault Zone, which could accommodate part of this $\sim 40\,\mathrm{m\,Myr^{-1}}$ of differential uplift, as suggested by the M_w 4.9 Teil earthquake surface rupture ~ 100 km to the northeast. The use of 13 more new burial ages for quartz-rich alluvium deposited in the four caves located in the central region of the Larzac plateau (2–3 km from the canyon edges) give unexpectedly younger ages by 1–3 Ma from the ones predicted by the conventional epigenic speleogenesis model in relation to the canyon incision. We conclude that the speleogenesis in the study area does not follow the widely accepted epigenic paradigm but is primarily due to headward erosion of previously altered rocks. Once the river cuts through a primokarst by deepening its canyon, the induced high water flow can evacuate the ghost rocks and quickly form new caves. Some of these caves can show several levels for which the timing of construction is only related to the time of the alteration of the rocks prior to the speleogenesis rather than being correlated to regional base level changes. We suggest that the previously proposed ghost rock process for large karst network genesis (Dubois et al., 2014; Quinif and Bruxelles, 2011) can also be applied at the scale of large limestone plateaus and could be the first stage of large void opening prior to the high water flow hydrodynamic phase.

Code availability. The code is still in development and will be made publicly available in the future. For now it can be directly requested from the corresponding author.

Data availability. The data used are provided as a Supplement and are available on the Karst3D database (2019, https://doi.org/10.15148/940c2882-49f1-49db-a97e-12303cace752).

Supplement. The supplement related to this article is available online at: https://doi.org/10.5194/esurf-12-679-2024-supplement.

Author contributions. OM, PV, DF, JFR, and JC performed the field work and sampling. OM, GC, DF, and TJ performed the sample preparation and measurement on the AMS. OM and PV performed the initial data analysis and draft of the paper. All authors discussed the result, the data analysis and commented on the paper.

Competing interests. The contact author has declared that none of the authors has any competing interests.

Disclaimer. Publisher's note: Copernicus Publications remains neutral with regard to jurisdictional claims made in the text, published maps, institutional affiliations, or any other geographical representation in this paper. While Copernicus Publications makes every effort to include appropriate place names, the final responsibility lies with the authors.

Acknowledgements. We thank Charles Mifsud, Krista Stevens and Steve Kotevski for their assistance during the sample processing and Klaus Wilcken for assistance in some of the earlier AMS measurements. We also thanks Yann Guessard, Laurent Bruxelles, Michel Roux and Ludovic Leterme for the identification of cave infilling or their help during sampling. We acknowledge financial support from ANSTO portal AP12168 and from the Australian Government for the Centre for Accelerator Science at ANSTO through the National Collaborative Research Infrastructure Strategy (NCRIS). We are grateful to Philippe Audra, Régis Braucher and Fritz Schlunegger for their helpful reviews.

Financial support. Oswald Malcles has benefited from a doctoral grant provided by the French Ministère de l'Éducation Nationale de l'Enseignement Supérieur et de la Recherche and an AINSE–ANSTO French Embassy Research Internship (SAAFE) portal. This research has partially been supported by ANSTO portal project AP12168.

Review statement. This paper was edited by Richard Gloaguen and reviewed by Philippe Audra, Fritz Schlunegger, and Regis Braucher.

References

Alabouvette, B., Arrondeau, J. P., Aubague, M., Bodeur, Y., Dubois, P., Mattei, J., Paloc, H., and Rancon, J. Ph.: Carte Géologique de la France à 1/50 000 Le Caylar, Edition BRGM, http://ficheinfoterre.brgm.fr/Notices/0962N.pdf (last access: 23 April 2024), 1988.

Audra, P. and Palmer, A. N.: 6.17 The Vertical Dimension of Karst: Controls of Vertical Cave Pattern, in: Treatise on Geomorphology, Elsevier, 186–206, https://doi.org/10.1016/B978-0-12-374739-6.00098-1, 2013.

Balco, G.: Production rate calculations for cosmic-ray-muon-produced ^{10}Be and ^{2}6Al benchmarked against geological calibration data, Quat. Geochronol., 39, 150–173, https://doi.org/10.1016/j.quageo.2017.02.001, 2017.

Balco, G. and Rovey, C. W.: An isochron method for cosmogenic-nuclide dating of buried soils and sediments, Am. J. Sci., 308, 1083–1114, https://doi.org/10.2475/10.2008.02, 2008.

Braucher, R., Bourlès, D., Merchel, S., Vidal Romani, J., Fernadez-Mosquera, D., Marti, K., Léanni, L., Chauvet, F., Arnold, M., Aumaître, G., and Keddadouche, K.: Determination of muon attenuation lengths in depth profiles from in situ produced cosmogenic nuclides, Nucl. Instrum. Meth. B, 294, 484–490, https://doi.org/10.1016/j.nimb.2012.05.023, 2013.

Camus, H.: Vallée et réseaux karstiques de la bordure carbonatée sud-cévenole, Relation avec la surrection, le volcanisme et les 45 paléoclimats, Thèse de doctorat, Université Bordeaux, Bordeaux, 3, 692 pp., 2003.

Child, D., Elliott, G., Mifsud, C., Smith, A. M., and Fink, D.: Sample processing for earth science studies at ANTARES, Nucl. Instrum. Meth. B, 172, 856–860, https://doi.org/10.1016/S0168-583X(00)00198-1, 2000.

Chmeleff, J., von Blanckenburg, F., Kossert, K., and Jakob, D.: Determination of the ^{10}Be half-life by multicollector ICP-MS and liquid scintillation counting, Nucl. Instrum. Meth. B, 268, 192–199, https://doi.org/10.1016/j.nimb.2009.09.012, 2010.

Dubois, C., Quinif, Y., Baele, J. M., Barriquand, L., Bini, A., Bruxelles, L., Dandurand, G., Havron, C., Kaufmann, O., Lans, B., Maire, R., Martin, J., Rodet, J., Rowberry, M. D., Tognini, P., and Vergari, A.: The process of ghost-rock karstification and its role in the formation of cave systems, Earth Sci. Rev., 131, 116–148, https://doi.org/10.1016/j.earscirev.2014.01.006, 2014.

Dubois, C., Bini, A., and Quinif, Y.: Karst morphologies and ghostrock karstification, Geomorphologie, 28, 13–31, https://doi.org/10.4000/geomorphologie.16327, 2022.

Dandurand, G., Quinif, Y., Guendon, J.-L., and Gruneisen, A.: Sources vauclusiennes et fantômes de roche, Karstologia, 74, 31–46, 2019.

Dunai, T. J.: Cosmogenic Nuclides: Principles, Concepts and Applications in the Earth Surface Sciences, Cambridge University Press, 198 pp., ISBN 10 0511804512, 2010.

Ford, D. and Williams, P.: Karst Hydrogeology and Geomorphology, Ford/Karst Hydrogeology and Geomorphology, West Sussex, England, John Wiley & Sons Ltd., https://doi.org/10.1002/9781118684986, 2007.

Granger, D. E. and Muzikar, P. F.: Dating sediment burial with in situ-produced cosmogenic nuclides: theory, techniques, and limitations, Earth Planet. Sc. Lett., 188, 269–281, https://doi.org/10.1016/S0012-821X(01)00309-0, 2001.

Granger, D. E., Kirchner, J. W., and Finkel, R. C.: Quaternary downcutting rate of the New River, Virginia, measured from differential decay of cosmogenic ^{26}Al and ^{10}Be in cave-deposited alluvium, Geology, 25, 107, https://doi.org/10.1130/0091-7613(1997)025<0107:QDROTN>2.3.CO;2, 1997.

Granger, D. E., Fabel, D., and Palmer, A. N.: Pliocene−Pleistocene incision of the Green River, Kentucky, determined from radioactive decay of cosmogenic ^{26}Al and ^{10}Be in Mammoth Cave sediments, GSA Bulletin, 113, 825–836, 2001.

Harmand, D., Adamson, K., Rixhon, G., Jaillet, S., Losson, B., Devos, A., Hez, G., Calvet, M., and Audra, P.: Relationships between fluvial evolution and karstification related to climatic, tectonic and eustatic forcing in temperate regions, Quaternary Sci. Rev., 166, 38–56, https://doi.org/10.1016/j.quascirev.2017.02.016, 2017.

Haeuselmann, P., Granger, D. E., Jeannin, P.-Y., and Lauritzen, S.-E.: Abrupt glacial valley incision at 0.8 Ma dated from cave deposits in Switzerland, Geology, 35, 143–146, https://doi.org/10.1130/G23094A, 2007.

Karst3D Team: KARST3D, OSU OREME [data set], https://doi.org/10.15148/940c2882-49f1-49db-a97e-12303cace752, 2019.

Klimchouk, A.: Speleogenesis, Hypogenic, in: Encyclopedia of Caves, Elsevier, 748–765, https://doi.org/10.1016/B978-0-12-383832-2.00110-9, 2012.

Klimchouk, A.: The Karst Paradigm: Changes, Trends and Perspectives, Acta Carsologica/Karsoslovni Zbornik, 44, 289–313, https://doi.org/10.3986/ac.v44i3.2996, 2015.

Klimchouk, A.: Types and Settings of Hypogene Karst, in: Hypogene Karst Regions and Caves of the World, edited by: Klimchouk, A., N. Palmer, A., De Waele, J., S. Auler,

A., and Audra, P., Springer International Publishing, Cham, https://doi.org/10.1007/978-3-319-53348-3, 2017.

Kohl, C. P. and Nishiizumi, K.: Chemical isolation of quartz for measurement of in-situ-produced cosmogenic nuclides, Geochim. Cosmochim. Ac., 56, 3583–3587, https://doi.org/10.1016/0016-7037(92)90401-4, 1992.

Korschinek, G., Bergmaier, A., Faestermann, T., Gerstmann, U. C., Knie, K., Rugel, G., Wallner, A., Dillmann, I., Dollinger, G., Lierse von Gostomski, Ch., Kossert, K., Maiti, M., Poutivtsev, M., and Remmert, A.: A new value for the half-life of ^{10}Be by Heavy-Ion Elastic Recoil Detection and liquid scintillation counting, Nucl. Instrum. Meth. B, 268, 187–191, https://doi.org/10.1016/j.nimb.2009.09.020, 2010.

Kuhn, T. S.: he structure of scientific revolutions, University of Chicago, Chicago, 4 Edn., ISBN 13 978-0-226-45812-0, 1962.

Lal, D.: Cosmic ray labeling of erosion surfaces: in situ nuclide production rates and erosion models, Earth Planet. Sc. Lett., 104, 424–439, 1991.

Malcles, O., Vernant, P., Chéry, J., Camps, P., Cazes, G., Ritz, J.-F., and Fink, D.: Determining the Plio-Quaternary uplift of the southern French Massif Central; a new insight for intraplate orogen dynamics, Solid Earth, 11, 241–258, https://doi.org/10.5194/se-11-241-2020, 2020a.

Malcles, O., Vernant, P., Chéry, J., Ritz, J.-F., Cazes, G., and Fink, D.: Âges d'enfouissement, fantômes de roches et structuration karstique, cas de la vallée de la Vis (Sud de la France), Géomorphologie: relief, processus, environnement, 26, 255–264, https://doi.org/10.4000/geomorphologie.15043, 2020b.

Nishiizumi, K., Imamura, M., Caffee, M. W., Southon, J. R., Finkel, R. C., and McAninch, J.: Absolute calibration of ^{10}Be AMS standards, Nucl. Instrum. Meth. B, 258, 403–413, https://doi.org/10.1016/j.nimb.2007.01.297, 2007.

Palmer, A. N.: Cave Geology, Cave Books, Revised edition, 454 pp., ISBN 13 978-0939748815, 2017.

Quinif, Y.: Fantômes de roche et fantômisation: essai sur un nouveau paradigme en karstogénèse, edited by: Quinif, Y., Mons, 190 pp., ISBN 13 978-2-87509-016-4, 2010.

Quinif, Y., and Bruxelles, L.: L'altération de type "fantôme de roche": processus, évolution et implications pour la karstification, Géomorphologie: relief, processus, environnement, 17, 349–358, https://doi.org/10.4000/geomorphologie.9555, 2011.

Ritz, J.-F., Baize, S., Ferry, M., Larroque, C., Audin, L., Delouis, B., and Mathot, E.: Surface rupture and shallow fault reactivation during the 2019 M_{w} 4.9 Le Teil earthquake, France, Commun. Earth Environ., 1, 10, https://doi.org/10.1038/s43247-020-0012-z, 2020.

Rodet, J.: The primokarst, former stages of karstification, or how solution caves can born, Geologic Belgica, 17, 58–65, 2014.

Sartégou, A., Mialon, A., Thomas, S., Giordani, A., Lacour, Q., Jacquet, A., André, D., Calmels, L., Bourlès, D., Bruxelles, L., Braucher, R., Leanni, L., and Aster Team: When TCN meet high school students: deciphering western Cévennes landscape evolution (Lozère, France) using TCN on karstic networks, 4th Nordic Workshop on Cosmogenic Nuclides, 4–6 June 2018, https://doi.org/10.13140/RG.2.2.17907.37921, 2018.

Schmidt, V. A.: The paleohydrology of Laurel Caverns, Pennsylvania, Proceedings of the 4th Conference on Karst Geology and Hydrology, Morgantown, edited by: Rauch, H. W. and Werner, E., West Virginia Geological and Economic Survey, 123–128, 1974.

Séranne, M., Camus, H., Lucazeau, F., Barbarand, J., and Quinif, Y.: Polyphased uplift and erosion of the Cévennes (southern France). An example of slow morphogenesis, B. Soc. Géol. Fr., 173, 97–112, https://doi.org/10.2113/173.2.97, 2002.

Stock, G. M., Granger, D. E., Sasowsky, I. D., Anderson, R. S., and Finkel, R. C.: Comparison of U–Th, paleomagnetism, and cosmogenic burial methods for dating caves: Implications for landscape evolution studies, Earth Planet. Sc. Lett., 236, 388–403, https://doi.org/10.1016/j.epsl.2005.04.024, 2005.

Vernet, J., Mercier, N., Bazile, F., and Brugal, J.: Travertins et terrasses de la moyenne vallée du Tarn à Millau (Sud du Massif Central, Aveyron, France): datations OSL, contribution à la chronologie et aux paléoenvironnements, Quaternaire, 19, 3–10, https://doi.org/10.4000/quaternaire.1422, 2008.

Wells, D. L. and Coppersmith, Kevin, J.: New empical relationship between magnitude, rupture length, rupture width, rupture area, and surface displacement, B. Seismol. Soc. Am., 84, 974–1002, 1994.

Wilcken, K. M., Fujioka, T., Fink, D., Fülöp, R. H., Codilean, A. T., Simon, K., Mifsud, C., and Kotevski, S.: SIRIUS Performance: ^{10}Be, ^{26}Al and ^{36}Cl measurements at ANSTO, Nucl. Instrum. Meth. B, 455, 300–304, https://doi.org/10.1016/j.nimb.2019.02.009, 2019.